2014 IEEE International Conference on Robotics & Automation (ICRA)
Hong Kong Convention and Exhibition Center
May 31 - June 7, 2014. Hong Kong, China

Real-time Trajectory Tracking for Externally Loaded Concentric-tube Robots

Ran Xu†, Ali Asadian†, Seyed Farokh Atashzar†, and Rajni V. Patel*

Abstract— **Concentric-tube robots can offer a suitable compromise between force and curvature control. In a previous study by the authors, a real-time trajectory tracking scheme for an unloaded concentric-tube robot was developed. One of the practical barriers to the use of a concentric-tube robot in medical applications is compensation for the impact of environmental forces which can cause drastic deterioration in tracking performance. In this paper, by modifying the robot's forward kinematics and Jacobian, a new method is developed to facilitate tip tracking in real-time while accounting for an external load at the robot's tip. By considering the tip deflection resulting from the external load, a novel dual-layer control architecture is proposed to compensate for this deflection during trajectory tracking. In order to measure the force exerted on the tip position of the robot, a new technique is proposed that can move the sensing system from the distal tip to the proximal base. Experimental results are given to illustrate the effectiveness of the proposed method.**

I. INTRODUCTION

A concentric-tube robot as a subset of continuum robots is composed of a sequence of telescoping pre-curved elastic tubes inserted one inside the next. In this flexible robotic structure, axial rotation and translation of individual tubes with respect to each other can generate 3D curvatures. Thus, the shape of the robot can be controlled in order to guide it inside lumens, natural orifices, and other anatomical organs in a variety of medical applications specially involving unreachable or confined surgical sites.

Accurate position control of surgical instruments is a vital need in Robotics-Assisted Minimally Invasive Surgery (RAMIS); however the small size of the incision reduces the robot rigidity and, as a result, challenges positioning accuracy. As is known, flexible surgical tools (such as surgical needles [1]) have been widely used in percutaneous minimally invasive interventions. However, complex and inaccurate kinematics modeling of flexible/continuum mechanisms has imposed limitations on accurate control of the tip motion in RAMIS. This topic has been the subject of recent publications for concentric tube robots [2], [3], and is explored further in this study.

Modeling the shape of concentric-tube robots has evolved over the last few years. Historically, a variety of mechanical phenomena, e.g., bending [4], torsion [2] [5], and friction between the tubes [6] have been gradually taken into account to improve modeling accuracy. It has been shown that the assumption of zero external load in kinematic modeling can cause considerable error in estimating the robot configuration [7]. To deal with this issue, in [7] and [8] the forward kinematics of the robot are modified to include the effects of external loading. However, most of the developed models are mathematically complex and computationally expensive. To achieve a good balance between computational efficacy and numerical accuracy, the authors proposed a fast torsionally-compliant model [9], which was later utilized to develop a feasible strategy for real-time tip tracking in free motion [3]. Human-in-the-loop architecture was developed in [2], and [10] respectively using an inverse kinematics scheme and an inverse Jacobian technique (with singularity avoidance) as local controllers. Implementation of Magnetic Resonance Imaging based position control (utilizing inverse kinematics) is given in [11]. In addition, more advanced control architectures such as stiffness control [12] have been recently studied in the literature.

In this paper for the first time, the problem of real-time position control in the presence of undesirable robot deflection is studied. The deflection is caused by: (a) variations in external loading, and (b) alteration of kinematic behavior of the robot in the presence of external forces. The ultimate goal is to navigate the robot accurately regardless of external disturbances. This feature is important in medical applications, where the targeting accuracy strongly correlates with the performance of the administered therapy. For this goal, deflection of a concentric-tube robot in the presence of external disturbances is estimated; then, the desired trajectory is reshaped using the estimated robot deflection in order to compensate for the effect of varying loading. For this purpose, the interaction force between the robot tip position and environment should be used in the proposed control architecture. In this paper a new scheme is proposed that uses force sensors at the proximal end (close to the driving unit) of the robot. This removes the need for measuring the force at the distal end (close to the robot's tip position) while compensating for the internal forces between the tubes. This feature is motivated by the fact that having a sensor close to the robot's tip is not very feasible in practical application.

†R. Xu, A. Asadian, and S.F. Atashzar contributed equally to the presented work. The authors are with Canadian Surgical Technologies and Advanced Robotics (CSTAR), Lawson Health Research Institute, London, ON N6A 5A5, Canada, and with the Dept. of Electrical and Computer Engineering, Western University, London, ON N6A 5B9, Canada. R.V. Patel is also with the Department of Surgery, Western University (emails: rxu25@uwo.ca, aasadian@uwo.ca, satashza@uwo.ca, rvpatel@uwo.ca). Partial financial support was provided by the following grants awarded to R.V. Patel: the Natural Sciences and Engineering Research Council (NSERC) of Canada, grant RGPIN1345, the NSERC Collaborative Research and Training Experience (CREATE) program grant #371322-2009 on Computer-Assisted Medical Interventions (CAMI), and the Canada Research Chairs Program and a Canada Foundation for Innovation grant. Partial financial support for R. Xu was also provided by a postgraduate scholarship from the Peoples Republic of China.

*Project leader.

II. FORWARD KINEMATICS AND JACOBIAN IN THE PRESENCE OF AN EXTERNAL POINT LOAD

Modeling of a concentric-tube robot under an external load has been the subject of several research papers [7], [8]. Existing models include distributed wrench to mimic robot-environment interaction, and apply lumped wrench as boundary conditions to the governing set of equations. However, due to the limitations of sensing technology, it is not feasible to obtain accurate force and torque information along the robot's shaft, and update the equations. Computational complexity is also a typical barrier to real-time implementation in existing techniques. In the following section, the fast forward kinematics and the resultant Jacobian [3] are introduced so as to incorporate the impact of the external load for real-time trajectory tracking.

A. Fast Torsionally Compliant Model for the Loaded Robot

According to Cosserat rod theory, a single elastic rod obeys the equations of equilibrium [8]:

$$\dot{n}(s) + f(s) = 0 \tag{1}$$

$$\dot{m}(s) + \dot{r}(s) \times n(s) + l(s) = 0 \tag{2}$$

where $m(s)$ and $n(s)$ are the moment and stress vectors in the cross-section in terms of the length variable s; $f(s)$ and $l(s)$ are respectively the distributed force and torque along the rod; and $r(s) = [x(s)\ y(s)\ z(s)]^T$ is the position vector for a given cross-section represented in the world frame as shown in Fig. 1(a). For an assembly of q tubes, equations (1) and (2) are extended as follows in which the subscript i denotes the tube number:

$$\sum_{i=1}^{q} \big(\dot{n}_i(s) + f_i(s)\big) = 0 \tag{3}$$

$$\sum_{i=1}^{q} \big(\dot{m}_i(s) + \dot{r}_i(s) \times n_i(s) + l_i(s)\big) = 0 \tag{4}$$

Defining $\dot{M}(s) = \sum_{i=1}^{q} \dot{m}_i(s)$ as the derivative of the net moment, and knowing that in the absence of the external torque, we have $\sum_{i=1}^{q} l_i(s) = 0$, equation (4) is rewritten as

$$\dot{M}(s) = -\dot{r}(s) \times F_{ext} \tag{5}$$

where $F_{ext} = \sum_{i=1}^{q} n_i(s)$ represents the external point force. Thus, the modified forward kinematics which accounts for the external point load is obtained by adding (5) to the unloaded structure introduced in [3]. The new model is formulated as shown below:

$$\dot{u}_{iz}(s) = \frac{k_{ix}(s)}{k_{iz}(s)}\big(u_{ix}(s)\hat{u}_{iy}(s) - u_{iy}(s)\hat{u}_{ix}(s)\big) \tag{6}$$

$$\dot{\theta}_1(s) = \frac{u_{ix}(s)cos\theta_{i3}(s) - u_{iy}(s)sin\theta_{i3}(s)}{cos\theta_2(s)} \tag{7}$$

$$\dot{\theta}_2(s) = u_{ix}(s)sin\theta_{i3}(s) + u_{iy}(s)cos\theta_{i3}(s) \tag{8}$$

$$\dot{\theta}_{i3}(s) = u_{iz}(s) - \dot{\theta}_1(s)sin\theta_2(s) \tag{9}$$

$$\dot{x}(s) = sin\theta_2(s) \tag{10}$$

$$\dot{y}(s) = -sin\theta_1(s)cos\theta_2(s) \tag{11}$$

$$\dot{z}(s) = cos\theta_1(s)cos\theta_2(s) \tag{12}$$

$$\dot{M}(s) = -\dot{r}(s) \times F_{ext} \tag{13}$$

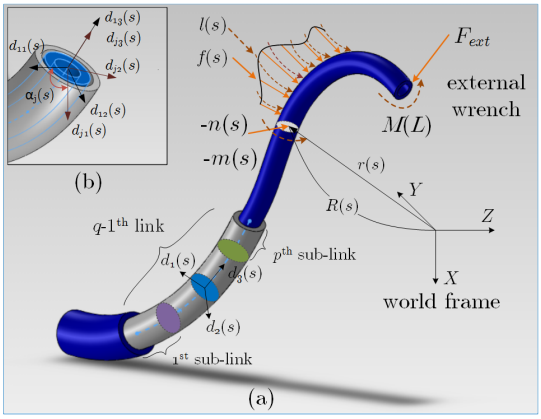

Fig. 1. (a) A loaded concentric-tube robot consisting of q links or tubes each of which is composed of p sub-links [3]; (b) the robot's cross section showing coordinate frames associated with the 1$^{\text{st}}$ and the j^{th} tubes [9].

in which, $\hat{u}_i$ is the initial curvature value while u_i represents its value after conformation. θ_1 and θ_2 are the first and second Euler angles shared by all tubes; θ_{i3} stands for the 3$^{\text{rd}}$ Euler angle of the i^{th} tube's cross-section.

For modeling the kinematics of unloaded concentric-tube robots [9], it was assumed that at any cross section, bending moment from all tubes were balanced, and so the net moment was zero. To add the impact of the external load to the model, the curvatures in the X and Y directions are updated in the following manner:

$$\begin{bmatrix} u_{ix}(s) \\ u_{iy}(s) \end{bmatrix} = \Big(\big(\sum_{j=1}^{q} K_j \big)^{-1} R_Z^T\big(\theta_{i3}(s) - \theta_{13}(s)\big) \times \sum_{j=1}^{q} R_Z^T\big(\theta_{j3}(s) - \theta_{13}(s)\big) K_j \begin{bmatrix} \hat{u}_{jx}(s) \\ \hat{u}_{jy}(s) \end{bmatrix} + R_i^T M(s) \Big) \tag{14}$$

in which, $K_j = diag(k_{jx}, k_{jy}, k_{jz})$ refers to the stiffness matrix calculated from Young's modulus and moment of inertia. The transformation between the body frames of the 1$^{\text{st}}$ and the j$^{\text{th}}$ tubes is also represented by a pure rotation denoted by the matrix $R_Z(\alpha_j(s))$ in (14). Herein, $\alpha_j(s) = \theta_{j3}(s) - \theta_{13}(s)$ in which $1 \leq j \leq q$. In addition, R_i is the rotation matrix between the body frame of the i^{th} tube with respect to the world frame. For more details, see Fig. 1(b).

Finally, equations (6)-(14) describe the forward kinematics of the concentric-tube robot in the presence of an external point load on the shaft. Note that except for the curvature variables which are expressed in the body frame $\{d_1(s), d_2(s), d_3(s)\}$, other variables are represented in the world frame shown in Fig. 1. A linearization technique is employed at this point to derive a closed-form solution for the robot's forward kinematics. Applying a first-order Taylor series expansion to this nonlinear mapping, we have:

$$\begin{bmatrix} \dot{u}_{iz}(s) \\ \dot{\Theta}(s) \\ \dot{r}(s) \\ \dot{M}(s) \end{bmatrix} = \begin{bmatrix} g_{11} & g_{12} \\ g_{21} & g_{22} \\ g_{31} & g_{32} \\ g_{41} & g_{42} \end{bmatrix} \begin{bmatrix} 1 \\ s \end{bmatrix} \tag{15}$$

in which $\Theta(s) = [\theta_1(s)\ \theta_2(s)\ \theta_{i3}(s)]^T$. The sought piecewise solution is therefore obtained by integration of (15) with

respect to s.

$$\begin{bmatrix} u_{iz}(s) \\ \Theta(s) \\ r(s) \\ M(s) \end{bmatrix} = \begin{bmatrix} g_{11} & g_{12} \\ g_{21} & g_{22} \\ g_{31} & g_{32} \\ g_{41} & g_{42} \end{bmatrix} \begin{bmatrix} s \\ \frac{1}{2}s^2 \end{bmatrix} + \begin{bmatrix} u_{iz}(0) \\ \Theta(0) \\ r(0) \\ M(0) \end{bmatrix} \tag{16}$$

Subsequently, the robot's arm is divided into links and small sub-links (see Fig. 1(a)), and the kinematic equations for each segment are derived as described in this section. Successive approximation is eventually employed to find the forward kinematics of the full robot, namely, F. The entire procedure has been outlined in detail in [3].

B. The Modified Jacobian for the Loaded Robot

Once the closed-form solution of each sub-link is obtained, the forward kinematics $\tilde{F}$ are differentiated to derive the associated Jacobian matrix $\tilde{J}$. Compared with the unloaded concentric-tube robot [3], in the presence of the external point load, one more vector variable, i.e., M, is introduced in the vector Θ. Let us define,

$$\tilde{J}_{g1} = \begin{bmatrix} \frac{\partial \tilde{F}}{\partial u_{iz}(0)} & \frac{\partial \tilde{F}}{\partial \Theta(0)} & \frac{\partial \tilde{F}}{\partial P(0)} & \frac{\partial \tilde{F}}{\partial M(0)} \end{bmatrix} \tag{17}$$

$$\tilde{J}_{g2} = \begin{bmatrix} \frac{\partial \tilde{F}}{\partial H}\frac{\partial H}{\partial P_1} & \frac{\partial \tilde{F}}{\partial H}\frac{\partial H}{\partial P_2} & \dots & \frac{\partial \tilde{F}}{\partial H}\frac{\partial H}{\partial P_q} \end{bmatrix} \tag{18}$$

where P_j represents the position of the proximal end of the j^{th} tube along the z-axis. Moreover, H is the mapping which projects the P_j elements to each sub-link's length. Except for the last sub-link in each link, we have:

$$\tilde{J} = \begin{bmatrix} \tilde{J}_{g1} & 0 \\ 0 & I_{q\times q} \end{bmatrix} \text{ otherwise, } \begin{bmatrix} \tilde{J}_{g1} & \tilde{J}_{g2} \\ 0 & I_{q\times q} \end{bmatrix} \tag{19}$$

Finally, the relationship between the velocities of the robot's distal and proximal ends is established as shown below in which L is the length of the assembled robot:

$$\begin{aligned} &[\dot{u}_{iz}(L)\ \dot{\Theta}(L)\ \dot{r}(L)\ \dot{M}(L)]^T = \\ &\qquad J[\dot{u}_{iz}(0)\ \dot{\Theta}(0)\ \dot{r}(0)\ \dot{M}(0)]^T \end{aligned} \tag{20}$$

In (20), the robot's Jacobian J is obtained by multiplication of individual Jacobians $\tilde{J}$. This equation is part of an inverse Jacobian-based scheme for position/orientation control.

III. THE EFFECT OF EXTERNAL LOADING AND A DUAL-LAYER CONTROL APPROACH

In this section, the effect of external loading on the tip position is studied and a dual-layer control approach is proposed to minimize the impact of external disturbances on trajectory tracking. Needless to say, the forward kinematics of the robot are not only a function of the joint variables q but also of the external wrench w. The former was studied in section II-B. The effect of external loading in the position domain is called "deflection" in this paper. It should be noted that the analytical inverse kinematics in the presence of an external wrench has not yet been developed for concentric tube robots, due to the computational complexity. As a result, it is not possible to utilize a conventional inverse-kinematic controller in order to eliminate the effect of external loading and minimize the associated deflection.

In this section, a dual-layer controller consisting of an inner loop and an outer loop is developed for trajectory tracking in Cartesian space. In brief, the objective of the inner control loop is to make a new inverse model of the robot in the differential domain and remove the effect of deflection on the tip velocity. Then, the outer controller transforms the tracking from the velocity domain to the position domain, and alleviates the impact of system uncertainties.

A. The Inner Control Loop

Let us consider the forward differential model of the robot as shown below [13]:

$$\dot{X} = J(q,w)\dot{q} + C(q,w)\dot{w} \tag{21}$$

Here, C is the compliance matrix which correlates the derivative of the external wrench to the robot's tip velocity. Thus, the tip motion in Cartesian space $\dot{X}$ is expressed by (21) in which the dot denotes the time derivate and $C = \frac{\partial F}{\partial w}$. This shows that the external wrench influences the tip motion through two different mechanisms, namely, the Jacobian and compliance terms. In order to design a proper control scheme for rejecting the total effect of the external loading and to have a better insight over the kinematics of the deflection, the total deflection Δ_{total} can be calculated as:

$$\begin{aligned} &\Delta_{total} = \Delta_1 + \Delta_2 \\ &\text{where, } \Delta_1 = \int C(q,w)\dot{w}\, dt \\ &\qquad\quad \Delta_2 = \int \big(J(q,w) - J(q,0)\big)\dot{q}\, dt \end{aligned} \tag{22}$$

Therefore, equation (21) is rewritten as (23) which is called the Standard Total Deflection (STD) model. This representation is close to the standard conventional definition of arm flexibility in flexible-link manipulators [14], [15].

$$\dot{X} = J(q,0)\dot{q} + \dot{\Delta}_{total} \tag{23}$$

In the next step, the STD model is employed to design an inverse model-based scheme for the inner loop controller. To this end, the following alternatives (Type-I and Type-II) are proposed:

1) Kinematics-based Deflection Estimation and Cancellation (Type-I): Considering the proposed STD representation, the Type-I control rule (24) can be used to reject the external load.

$$\dot{q}_{des} = J(q,0)^{-1}(U_{int} - \hat{\dot{\Delta}}_{total}) \tag{24}$$

where U_{int} represents the controller's input signal and $\hat{\dot{\Delta}}_{total}$ is an estimation of the rate of change of the total deflection. $\hat{\dot{\Delta}}_{total}$ is calculated through numerical derivation of the robot's forward kinematics considering the loaded and unloaded conditions using the following relationship.

$$\hat{\dot{\Delta}}_{total} = \frac{d}{dt}\big(F(q,w) - F(q,0)\big) \tag{25}$$

Applying the Type-I control scheme, the robot's tip velocity $\dot{X}$ will converge to the input of the inner loop U_{int} which can be considered equal to the desired velocity in the velocity tracking mode. Consequently, the known nonlinear terms of the robot's model are eliminated, and the resulting dynamics will be an input-to-output linearized system, shown in (26).

$$\dot{X} = U_{int} \tag{26}$$

It is worth mentioning that due to several sources of uncertainty in the system, namely, those due to the erroneous

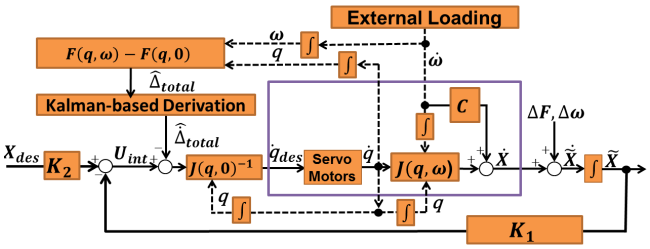

Fig. 2. Control block diagram for the proposed tracking algorithm.

forward kinematics model ΔF, force measurement errors $\Delta\omega$, and the robot's unmodeled dynamics, the actual tip velocity $\dot{\tilde{X}}$ does not exactly match the modeled tip velocity $\dot{X}$. This mismatch is denoted by δ as shown below:

$$\dot{\tilde{X}} = U_{int} + \delta \tag{27}$$

This relationship will be used to design the outer-loop controller which will be introduced later in this section. The proposed Type-I controller is considered as the inner-layer control scheme. Note that to benefit from this technique, a numerical derivation of the total deflection is required which might amplify the noise level. Thus, a Kalman filter is used to suppress the noise signal.

2) Tip Velocity Measurement for Deflection Cancellation (Type II): Revisiting (21), the deflection caused by the wrench derivative $\dot{\Delta}_1$ can be directly estimated without taking a numerical derivative and measuring the robot's tip velocity $\dot{X}_{meas}$ as shown below:

$$C(q,w)\dot{w} = \dot{\Delta}_1 \cong \dot{X}_{meas} - J(q,w)\dot{q} \tag{28}$$

Consequently, taking (28) and (21) into account, the Type-II inner-loop is realized by the following control law.

$$\dot{q}_{des} = J(q,w)^{-1}\Big(U_{int} - \big(\dot{X}_{meas} - J(q,w)\dot{q}\big)\Big) \tag{29}$$

Using the Type-II controller, the tip velocity measurement is used to cancel out the known nonlinearity of the robot which yields the same dynamics as those represented by (27). However, to realize this controller and reject the impact of a varying external disturbance, it is required to have access to the tip velocity at a sufficiently high sampling rate. In medical interventions, it is not always feasible to accurately register the tip velocity at a high rate. Electromagnetic tracking [9], [12], MRI [11], and ultrasound [16] have been widely utilized for position sensing. However, in most cases, neither accuracy nor the sampling rate is adequate to estimate velocity for accurate force rejection that has fast dynamics.

B. The Outer Control Loop

Using the inner control loop, an inverse model-based approach in the velocity domain was presented to deal with the deflection caused by the external load. In order to a) take advantage of the proposed technique in position domain and b) alleviate the effect of existing uncertainties, an outer control loop was added to shape the desired trajectory so as to adjust U_{int} toward tip positioning. It should be noted that since the majority of the system's nonlinearity was eliminated through implementing the inner loop at a high update rate, the proposed outer loop could be run at a low control rate. Consequently, an electromagnetic tracker providing the position information at a relatively low rate

TABLE I
PARAMETERS OF THE TWO-TUBE ROBOT

Tube pair	inner	outer
l (m)	0.150	0.012
L (m)	0.153	0.153
r (m)	0.250	0.250
Absolute stiffness value (Nm^2)	0.0413	0.048

was used in the outer loop to reject the undesirable effects of uncertainties while controlling the robot in position domain. The proposed outer loop controller is designed as follows:

$$U_{int} = -K_1\tilde{X} + K_2 X_{des} \tag{30}$$

where, K_1 and K_2 are the design factors for tuning the performance of the closed-loop system, and will be introduced later in this section. Combining (30) and (27), the system dynamics are rewritten as:

$$\tilde{X} = \frac{K_2}{S+K_1}X_{des} + \frac{\delta}{S+K_1} \tag{31}$$

in which, S is the Laplace operator. Considering the achieved first-order linear dynamics between the desired input X_{des} and the robot's tip position X, the outer loop can be designed such that the closed-loop behaves as a fast and stable system. Setting $K_1 = K_2 = k$, the tip tracking system acts as a low-pass filter which has a tunable bandwidth using the parameter k as well as a unity gain in steady-state. Increasing the value of k makes the system faster but more susceptible to high-frequency uncertainties and unmodelled dynamics represented by δ in (31). However, it will in turn increase the magnitude of the applied input signal to the inner loop U_{int}, and adversely influence the tracking performance by saturating the actuators. In summary, Fig. 2 depicts the block diagram for the two-layer closed-loop control system for tip tracking while rejecting or minimizing the impact of the external force.

IV. SIMULATION STUDY: TRAJECTORY TRACKING IN THE PRESENCE OF A TIP LOAD

We simulated a two-tube robot whose geometrical parameters and mechanical properties used for the study are listed in Table I. The lengths of the straight and curved sections of the tubes are represented by l and L, respectively, and the radius of curvature is denoted by r. These listed values correspond to the actual parameters of the robotic setup that is used in the experiments discussed in section V. The length of each sub-link was also assumed to be 10mm.

Fig. 3 illustrates the results of our simulation study in which a sinusoidal motion profile with an amplitude of 15mm and a frequency of 0.05Hz was applied as the desired trajectory to move the robot in the z direction. In this test, the robot remained stationary along other axes, and the tip load was also set to have the functional form $f_x = 0.2sin(2\pi \times 0.05t)$N. Four different control strategies were examined here: (a) the inverse Jacobian approach with no load compensation [3] where $\dot{q}_{des} = J(q,0)^{-1}\dot{X}_{des}$, (b) the inverse Jacobian approach with only load inclusion where $\dot{q}_{des} = J(q,w)^{-1}\dot{X}_{des}$. The compliance component, $C(q,w)\dot{\omega}$, is neglected in this architecture. (c) the inverse Jacobian approach using the inner loop controller defined

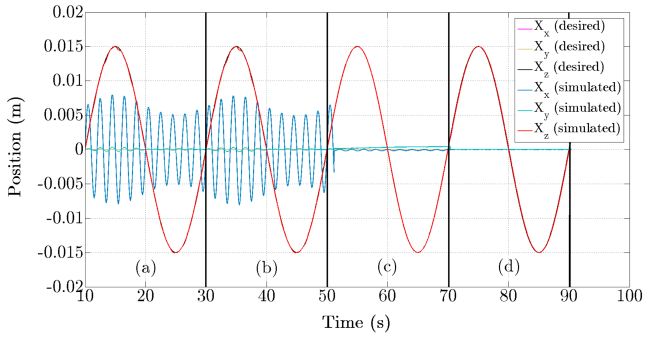

Fig. 3. Simulation of the tip position $X = [X_x\ X_y\ X_z]^T$ tracking using four control strategies: (a) unloaded Jacobian, (b) loaded Jacobian J, (c) loaded Jacobian J plus $\dot{\Delta}_{total}$, and (d) the dual-layer approach.

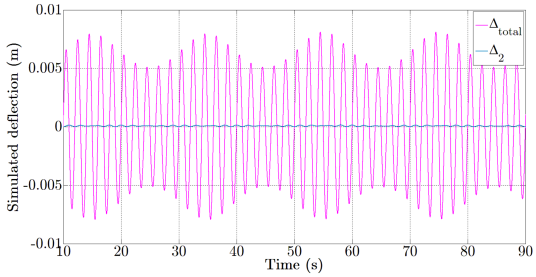

Fig. 4. Simulation of the tip deflection: comparison between the total deflection and the Jacobian-related component.

in (24). The external load is fully considered and the total deflection is compensated for in velocity mode. (d) the dual-layer control approach realized by combining equations (24) and (30). Here, the effects of loading, transformation from velocity mode to position mode, and uncertainties are taken into account.

As shown in Fig. 3, the pure Jacobian-based techniques, i.e., strategies (a) and (b), exhibited poor performance with a maximum tracking error of 7.9mm along the x-axis. Inclusion of the inner loop in the controller (strategy (c)) reduced the tracking error to a great extent. However, there was still a small drifting error which could be a result of the numerical uncertainties in integration and quantization. Finally, adding the outer loop to the control structure improved the performance, and demonstrated accurate tip tracking in the presence of the tip load. Fig. 4 shows the total deflection Δ_{total}, and the deflection component associated with the Jacobian part, Δ_2. As can be seen, Δ_1 dominates Δ_2; so most of the tip deflection in the case of loading is attributed to the compliance component, and that was why ignoring the term $C(q, w)\dot{\omega}$ in the force rejection algorithm led to poor tracking performance (see (a) and (b) in Fig. 3).

V. EXPERIMENTAL STUDY

A. Setup Description

The experimental evaluation was performed using a concentric-tube robot which consists of two superelastic Nitinol tubes (see Fig. 5). The inset plot in this figure shows the tubes each of which has a straight section at its proximal end followed by a distal section with a fixed curvature.

The outer tube was rotated with a rotary T-RS60 stage (Zaber) while the inner tube was respectively inserted and

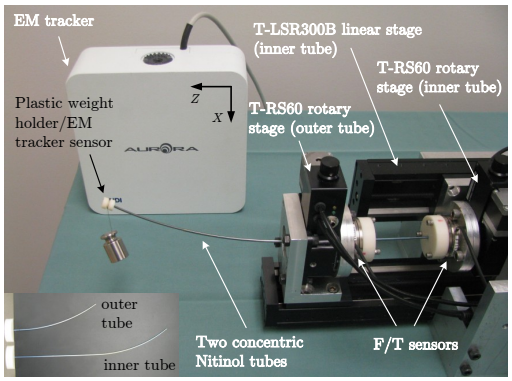

Fig. 5. A view of our concentric-tube robotic system.

rotated using a linear T-LSR300B stage and another rotary T-RS60 stage. An Aurora EM (electromagnetic) tracker (Northern Digital Inc.) was used for position sensing and validating the forward kinematics. For this purpose, a sensor coil of the EM tracker was attached to the robot's tip by a light plastic adaptor. Also, a metal weight (0.2-0.5N) was hung from the adapter using a rubber band to represent the external load. By lifting and dropping the weight, a varying force can be exerted on the robot. A multi-threaded application was developed using Microsoft® C++, MATLAB® and the QuaRC® Toolbox (Quanser Inc.). The inner control loop was updated at 500Hz, while the outer loop was sampled at 40Hz to measure tip position using EM tracking.

In order to update the force vector F_{ext} used in the model, a force sensing scheme is needed that provides inputs to the force rejection controller. Due to practical considerations and implementation issues (such as limited space on the tip of the robot, need for sensor sterilizability in an actual clinical application, etc.), it is not preferable to install conventional force sensors, such as strain gauges, directly on the distal end. In this paper, it is proposed to fuse the measurements of two 6-DOF (degrees-of-freedom) sensors (a two-tube configuration) mounted at the base of the two tubes. As a result, each sensor measures the forces acting on the corresponding tube. By fusing these measurements, the friction and internal interaction forces will cancel each other out and the residual will be the tip force. In this project two Nano43 ATI sensors were utilized.

B. Experimental Results

In the first study, the forward kinematics model introduced in Section II for the loaded model was validated. For this purpose, the outer tube was rotated a full turn at 3°/sec while the external tip load was set to be $f_x = 0.5$N. The measured tip position as well as the predicted values using the loaded model and the unloaded scheme (i.e., based on not considering the external load) [3] are shown in Fig. 6. The mean-squared errors (MSEs) using the loaded and unloaded schemes were 1.4mm and 9.5mm, respectively.

At this stage, experimental results for pure force rejection (regulation) and trajectory tracking are presented. In the first experiment, a time-varying external tip force with an amplitude smaller than 0.5N along the x-axis was applied.

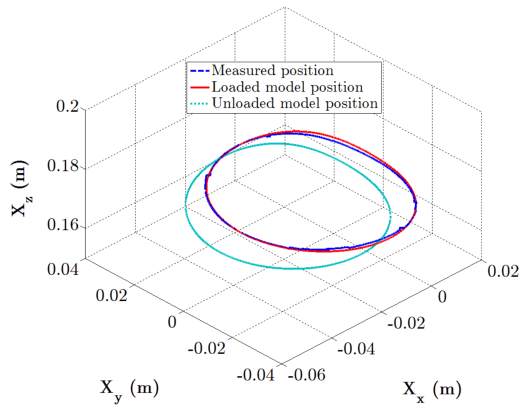

Fig. 6. Model validation: comparison between measured and predicted tip positions using loaded and unloaded schemes.

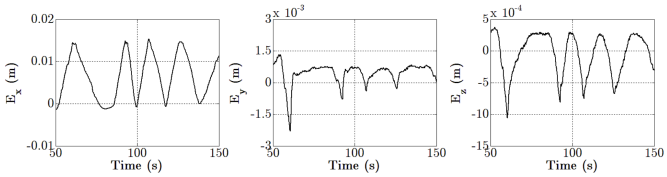

Fig. 7. Regulation using the inverse unloaded Jacobian approach [3].

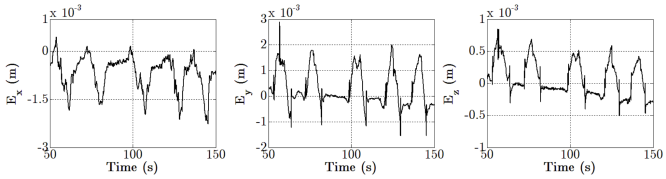

Fig. 8. Regulation using the proposed dual-layer control approach.

Our first objective was to regulate the robot so as to reject the external force while maintaining the same tip position. As observed in Fig. 7, the maximum positioning error was reported to be 15.5mm along the x-axis while only the robot's Jacobian was incorporated [3] in the control loop. The maximum tracking errors along the y- and z- axes were obtained as 2.3mm and 1.1mm, respectively. Next, the proposed control scheme outlined in section III was examined under the same test conditions in terms of tip force characteristics. Fig. 8 clearly demonstrates the capability of the two-layer approach to regulate the robot while the tracking error E was limited to $[2.2\ 2.8\ 0.8]^T$mm during the entire motion.

To perform trajectory tracking under a time-varying tip load, a sinusoidal reference signal with an amplitude of 10mm and frequency of 0.05Hz was applied to move the robot in the z direction. The tuning parameter of the outer loop k was set to be 2.5. The estimated tip force components, F_{ext}, from 100s to 200s are shown in Fig. 9, and Fig. 10 plots the tracking errors along the three axes. In this experiment, the maximum tip positioning error in the z direction was approximately 1.7mm. Since the external load had the largest magnitude along the x-axis, the robot was initially prone to considerable deflection in this direction; however, because of the proposed control scheme, perfect regulation limited E_x to $\pm$1mm .

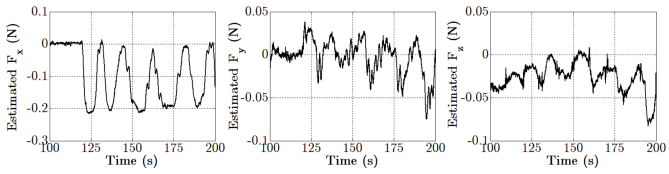

Fig. 9. Estimated tip force components during trajectory tracking using the proposed dual-layer control approach $F_{ext} = [F_x\ F_y\ F_z]^T$.

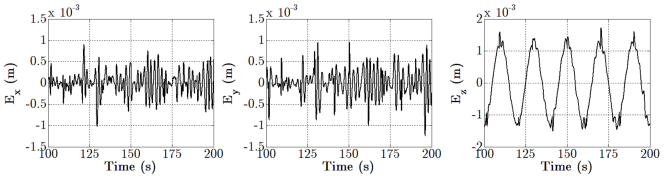

Fig. 10. Tip tracking error using the proposed dual-layer control approach.

REFERENCES

[1] A. Asadian, M.R. Kermani, and R.V. Patel, "A Novel Force Modeling Scheme for Needle Insertion Using Multiple Kalman Filters," *IEEE Trans. Instrum. Meas.*, vol. 61, no. 2, 2012, pp. 429-438.

[2] P. Dupont, J. Lock, B. Itkowitz, and E. Butler, "Design and Control of Concentric-tube Robots," *IEEE Trans. Robot.*, vol. 26, no. 2, pp. 209-225, 2010.

[3] R. Xu, A. Asadian, A. Naidu, and R.V. Patel, "Position Control of Concentric-tube Continuum Robots using a Modified Jacobian-based Approach," *In Proc. of IEEE Int. Conf. on Rob. Autom. (ICRA)*, 2013, pp. 5793-5798.

[4] P. Sears and P.E. Dupont, "A Steerable Needle Technology using Curved Concentric Tubes," *In Proc. of IEEE/RSJ Int. Conf. on Intel. Rob. Sys. (IROS)*, 2006, pp. 2850-2856.

[5] D.C. Rucker and R.J. Webster III, "Mechanics-based Modeling of Bending and Torsion in Active Cannulas," *In Proc. of IEEE RAS/EMBS Int. Conf. on Biomed. Rob. Biomech. (BioRob)*, 2007, pp.704-709.

[6] J. Lock and and P.E. Dupont, "Friction Modeling in Concentric Tube Robots," *In Proc. of IEEE Int. Conf. on Rob. Autom. (ICRA)*, 2011, pp. 11391146.

[7] J. Lock, G. Laing, M. Mahvash, and P.E. Dupont, "Quasistatic Modeling of Concentric Tube Robots with External Loads," *In Proc. of IEEE/RSJ Int. Conf. on Intel. Rob. Sys. (IROS)*, 2010, pp. 2325-2332.

[8] D.C. Rucker, B.A. Jones, and R.J. Webster III, "A Geometrically Exact Model for Externally Loaded Concentric-tube Continuum Robots," *IEEE Trans. Robot.*, vol. 26, no. 5, pp. 769-780, 2010.

[9] R. Xu and R.V. Patel, "A Fast Torsionally Compliant Kinematic Model of Concentric-tube Robots," *In Proc. of 34th IEEE EMBS Annu. Int. Conf.*, 2012, pp. 904-907.

[10] J. Burgner et al., "A Bimanual Teleoperated System for Endonasal Skull Base Surgery," *In Proc. of IEEE/RSJ Int. Conf. on Intel. Rob. Sys. (IROS)*, 2011, pp. 2517-2523.

[11] H. Su *et al.*, "A MRI-guided concentric tube continuum robot with piezoelectric actuation: a feasibility study," *In Proc. of IEEE Int. Conf. on Rob. Autom. (ICRA)*, 2012, pp. 1939-1945.

[12] M. Mahvash and P.E. Dupont, "Stiffness Control of Surgical Continuum Manipulators," *IEEE Trans. Robot.*, vol. 27, no. 2, pp. 334-345, 2011.

[13] D.C. Rucker, and R.J. Webster, "Computing Jacobians and Compliance Matrices for Externally Loaded Continuum Robots," *In Proc. of IEEE Int. Conf. on Rob. Autom. (ICRA)*, 2011, pp. 945-950.

[14] M. Moallem, R.V. Patel, and K. Khorasani, "Flexible-Link Robot Manipulators: Control Techniques and Structural Design," *in the Springer-Verlag Series: Lecture Notes in Control and Information Sciences*, vol. 257, 2000.

[15] S.F. Atashzar, M. Shahbaz, H.A. Talebi, and F. Towhidkhah, "A force observation method for tracking control of flexible-link manipulators," *Robotica*, vol. 31, no. 4, pp. 669-677, 2013.

[16] H. Ren, N.V. Vasilyev, and P.E. Dupont, "Detection of curved robots using 3D ultrasound," *In Proc. of IEEE/RSJ Int. Conf. on Intel. Rob. Sys. (IROS)*, 2011, pp. 2083-2089.